Dynamics of Bond Breaking in Ion Radicals. Mechanisms and Reactivity in the Reductive Cleavage of Carbon−Fluorine Bonds of Fluoromethylarenes

Claude P. Andrieux,[1a] Catherine Combellas,[1b] Frédéric Kanoufi,[1b] Jean-Michel Savéant,*[,1a] and André Thiébault*[,1b]

Contribution from the Laboratoire d'Electrochimie Moléculaire de l'Université Denis Diderot, Unité Associée au CNRS No 438, 2 place Jussieu, 75251 Paris Cedex 05, France, and the Laboratoire de Chimie et d'Electrochimie des Matériaux Moléculaires, ESPCI, 10 Rue Vauquelin, 75231 Paris Cedex 05, France

Received April 7, 1997[⊗]

Abstract: The reductive cleavage mechanism and reactivity of the carbon−fluorine bonds in fluoromethylarenes are investigated, in liquid ammonia and in DMF, by means of cyclic voltammetry and/or redox catalysis as a function of the number of fluorine atoms and of the structure of the aryl moiety. The reduction of the trifluoro compounds, eventually leading to complete defluorination, involves the di- and monofluoro derivatives as intermediates. Carbenes do not transpire along the reaction pathway. Application of the intramolecular dissociative electron transfer model allows the quantitative rationalization, in terms of driving force and intrinsic barrier, of the variation of the cleavage reactivity of the primary anion radical with the number of fluorine atoms and of the structure of the aryl moiety as well as with the solvating properties of the medium. When, related to the structural factors thus uncovered, the primary anion radical generates the di- and monofluoro intermediates far from the electrode surface, their reduction occurs homogeneously giving rise to an apparently direct six-electron process according to an internal redox catalysis mechanism. Conversely, with rapid cleavages, the reduction of the di- and monofluoro intermediates takes place at the electrode surface and the stepwise expulsion of the fluorides ions transpire in the cyclic voltammetric patterns.

Fluorocarbons are compounds of wide interest in view of their chemical and biological applications and of the importance of perfluoro polymers. For this reason, the electrochemical cleavage of carbon−fluorine bonds in fluorinated organic molecules has been the object of early interest.[2] In the case of perfluoro polymers, electron transfer cleavage of C−F may be envisaged as a route to a large variety of carbon materials as well as a first step of the derivatization of such polymers.[3]

Previous work has shown that the reduction of the three carbon−fluorine bonds often occurs simultaneously, the only product being the methyl derivative. In a few instances however, the CF_2H and CFH_2 intermediates have been found among the electrolysis products. Perusal of the available data leaves the impression that the simultaneous *versus* stepwise character of the reductive cleavage of the three carbon−fluorine bonds is a complex function of molecular structure and of the nature of the solvent. Electron-donating substituents on the phenyl ring of benzotrifluoride makes the reduction potential too negative for the C−F reductive cleavage to be investigated. This is the reason that the available data concern only benzotrifluorides with electron-withdrawing substituents or benzotrifluoride itself. Simultaneous cleavage of the three carbon−fluorine bonds occurs in the reduction of 4-carboxymethylbenzotrifluoride in methanol.[4] Cyclic voltammetric data indicate that the same is true in liquid ammonia for this compound and for the para-cyano derivative.[5] The CF_2H and CFH_2 intermediates have been identified among the reduction products of benzotrifluoride in *N*,*N*′-dimethylformamide (DMF) together with toluene. The respective yields vary with the electrolysis potential in a manner that is consistent with successive breaking of the C−F bonds. The intermediacy of the $C_6H_5CF_2^-$ carbanion in the reduction in DMF is confirmed by its trapping by electrophiles such as CO_2, acetone, or DMF itself.[6] The same is true for 4-fluorobenzotrifluoride in the same solvent.[6] The CFH_2 derivative was also found among the reduction product of ααα-trifluoroacetophenone in DMF,[7] whereas, in liquid NH_3, the cyclic voltammetric data point to a dimerization of the initially formed anion radical.[5]

So far, quantitative kinetic data are not available that would allow one to unravel the mechanism of the reductive cleavage of the three C−F bonds in trifluoromethylarenes. In the work reported below we have investigated in detail the direct or mediated electrochemical reduction of the 4-cyanotoluenes, **1′**, **1″**, and **1‴** where the α-carbon bears, one, two, and three fluorine atoms, respectively (see Chart 1). An important issue in the discussion of the reductive cleavage mechanism of trifluoromethyl compounds is to know whether it involves the intermediacy of the corresponding difluoro- and monofluoromethyl intermediates or whether it may involve carbene intermediates as previously observed with *gem*-polychloro and polybromo compounds.[8] Besides the reduction mechanism by

⊗ Abstract published in *Advance ACS Abstracts,* September 15, 1997.

(1) (a) Université Denis Diderot. (b) ESPCI.

(2) (a) Elving, P. J.; Leone, J. T. *J. Am. Chem. Soc.* **1957**, *79*, 1546. (b) Lund, H. *Acta Chem. Scand.* **1959**, *13*, 192. (c) Cohen, A. I.; Keeler, B. T.; Coy, N. H.; Yale, H. L. *Anal. Chem.* **1962**, *34*, 216.

(3) (a) Kavan, L. Electrochemical Carbonization of Fluoropolymers. In *Chemistry and Physics of Carbon*; Thrower, Ed.; Marcel Dekker: New York, 1991; pp 70−163. (b) Combellas, C.; Kanoufi, F.; Marzouk, H.; Thiébault, A. French Patent 9509726, 1995.

(4) (a) Coleman, J. P.; Gilde, H. G.; Utley, J. H. P.; Weedon, B. C. L. *J. Chem. Soc., Chem. Commun.* **1970**, 738. (b) Coleman, J. P.; Naser-uddin; Gilde, H. G.; Utley, J. H. P.; Weedon, B. C. L.; Eberson, L. *J. Chem. Soc., Perkin Trans. II* **1973**, 1903.

(5) Combellas, C.; Kanoufi, F.; Thiébault, A. *J. Electroanal. Chem.* **1996**, *407*, 195.

(6) Saboureau, C.; Troupel, M.; Sibille, S.; Périchon, J. *J. Chem. Soc., Chem. Comm.* **1989**, 1138.

(7) Stocker, J. H.; Jenevein, R. M. *J. Chem. Soc., Chem. Commun.* **1968**, 934.

S0002-7863(97)01094-9 CCC: $14.00

Chart 1

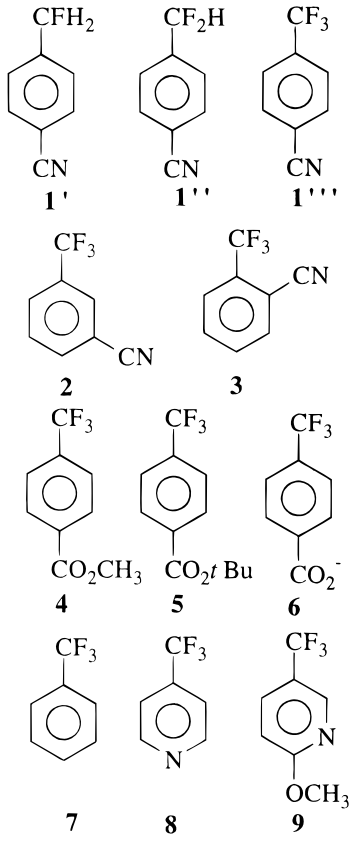

which the successive reductive cleavage of several C−F bonds occurs, the analysis of the kinetic results provides the standard potentials for the formation of each of the three anion radicals and their cleavage rate constants. The cleavage of an ion radical may be viewed as an intramolecular dissociative electron transfer. Based on this picture, a model of the dynamics of the reaction has been developed as an extension of the theory of dissociative electron transfer.[9] The model has been successfully applied to the cleavage of various series of frangible anion radicals.[9a,10] It is interesting to examine whether it is also able to rationalize the variation of the reductive cleavage reactivity of benzylic C−F bonds as a function of the number of fluorine atoms borne by the functional carbon and thus to explain the mechanism by which the three fluorine atoms are successively expelled from the molecule. All experiments were carried out both in *N*,*N*′-dimethylformamide (DMF) at 20 °C and in liquid ammonia at −38 °C in the purpose of examining the role of the nature of the solvent and of temperature in the reductive cleavage mechanism.

We have also measured (in liquid ammonia at −38 °C) the cleavage rate constants and standard potentials for the reductive cleavage of one C−F bond in a series of other trifluoromethyl derivatives where the aryl moiety is varied (**2**−**4** and **6**−**8** in Chart 1) in the purpose of examining the variation of the reductive cleavage reactivity with the help of the model mentioned above. The preliminary results previously obtained for the reductive cleavage of the first C−F bond in **5** and **9**[5] will also be rediscussed and used in the general discussion of the relationships between molecular structure and C−F cleavage reactivity.

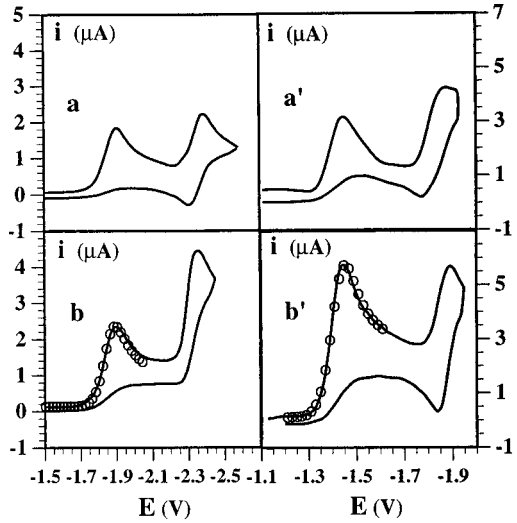

Figure 1. Reduction of **1**′ in DMF + 0.1 M *n*-Bu_4BF_4 at 20 °C (a, b) liquid NH_3 + 0.1 M KBr + 3 mM NH_4^+ at −38 °C and (a′, b′) in the absence (a, a′) and presence (b, b′) of an acid. [**1**′] = 1 mM (a, b), 3 mM (a′, b′). Scan rate: 0.2 V/s. [PhOH] = 10 mM (b), [NH_4Br] = 3 mM (b′). The potentials are referred to SCE in DMF and to 0.01 M Ag^+/Ag in liquid NH_3.

Results

Compound 1′. Figure 1 shows typical cyclic voltammograms obtained for the reduction of **1**′ in DMF and liquid NH_3. The cleavage of the C−F bond is expected to produce the 4-cyanotoluene carbanion which may react with acids present

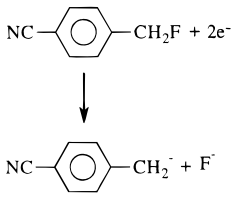

in the medium such as residual water leading to 4-cyanotoluene. It may also react with the starting material thus decreasing the electron stoichiometry below 2 and possibly generating several products which reduction is seen at more negative potentials. These side reactions may be eliminated by addition of an acid stronger than water as attested by the modification of the voltammograms upon addition of NH_4^+ in liquid NH_3 and of phenol in DMF (Figure 1). The electron stoichiometry then reaches 2, and the wave appearing at more negative potentials is that of 4-cyanotoluene. In liquid NH_3, the addition of a stoichiometric amount of NH_4Br is sufficient to raise the electron stoichiometry at the first wave up to 2. Under these conditions, the 4-cyanotoluene wave is a one-electron reversible wave. The depletion of NH_4^+ at the electrode surface caused by the protonation of the carbanion produced at the first wave thus leaves a concentration of acid which is insufficient to perturb the stability of the anion radical formed upon electron transfer to 4-cyanotoluene at the level of the second wave. In DMF, the addition of larger amounts of phenol is required to raise the electron stoichiometry at the first wave up to 2. Under these

(8) Petrosyan, V. E.; Niyazimbetv, M. E. *Russian Chem. Rev.* **1989**, *58*, 644.

(9) (a) Savéant, J. M. *J. Phys. Chem.* **1994**, *98*, 3716. (b) Savéant, J. M. *Acc. Chem. Res.* **1993**, *26*, 455. (c) Savéant, J. M. Dissociative Electron Transfer. In *Advances in Electron Transfer Chemistry*; Mariano, P. S., Ed.; JAI Press: New York, 1994; Vol. IV, pp 53−116. (d) Savéant, J. M. *Tetrahedron* **1994**, *50*, 10117−10165.

(10) (a) Adcock, W.; Andrieux, C. P.; Clark, C. I.; Neudeck, A.; Savéant, J.-M.; Tardy, C. *J. Am. Chem. Soc.* **1995**, *117*, 8285. (b) Andersen, M. L.; Mathivanan, N.; Wayner, D. D. M. *J. Am. Chem. Soc.* **1996**, *118*, 4871. (c) Andrieux, C. P.; Savéant, J.-M.; Tallec, A.; Tardivel, R.; Tardy, C. *J. Am. Chem. Soc.* **1996**, *118*, 9788. (d) Andrieux, C. P.; Savéant, J.-M.; Tallec, A.; Tardivel, R.; Tardy, C. *J. Am. Chem. Soc.*, in press.

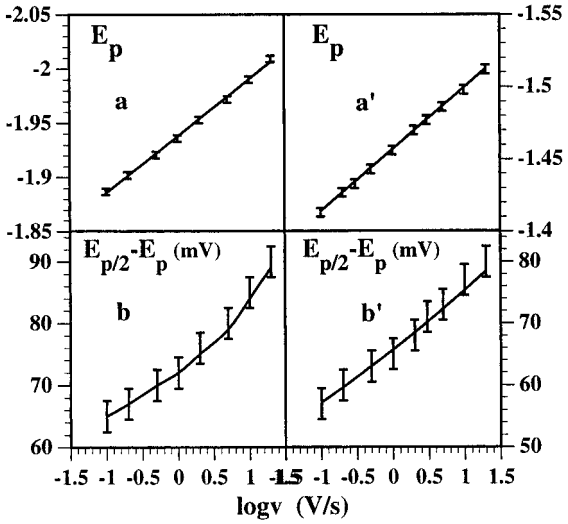

Figure 2. Variations of the peak potential (a, a′) and peak width (b, b′) for the reduction of 1 mM **1′** in DMF + 0.1 M *n*-Bu_4BF_4 + 10 mM PhOH at 20 °C (a, b) and of 3 mM **1′** in liquid NH_3 + 0.1 M KBr + 3 mM NH_4^+ at −38 °C (a′, b′). The potentials are referred to SCE in DMF and to 0.01 M Ag^+/Ag in liquid NH_3. The solid lines represent the fitting of the experimental data.

Scheme 1

$$ArCH_2F + e^- \underset{}{\overset{E^0_{1'},\, k_{S,1'},\, \alpha_{1'}}{\rightleftharpoons}} ArCH_2F^{\bullet -} \qquad (0)$$

$$ArCH_2F^{\bullet -} \xrightarrow{k_{1'}} ArCH_2^{\bullet} + F^- \qquad (1)$$

$$ArCH_2^{\bullet} + e^- \rightleftharpoons ArCH_2^- \qquad (2)$$

$$ArCH_2^{\bullet} + ArCH_2F^{\bullet -} \longrightarrow ArCH_2^- + ArCH_2F \qquad (2')$$

conditions, there is enough proton donor present in the diffusion layer to rapidly protonate the anion radical formed upon electron transfer to 4-cyanotoluene at the level of the second wave and thus to make it a two-electron irreversible wave.

The first cyclic voltammetric wave remains irreversible up to scan rates as large as 1000 V/s. The variations of the peak potential, E_p, and of the peak width, $E_{p/2} - E_p$, with the scan rate, v, (Figure 2) reveal that the reaction is jointly governed by the cleavage step (rate constant: $k_{1'}$) and the electrode electron transfer step ($E^0_{1'}$, $k_{S,1'}$ $\alpha_{1'}$, standard potential, standard rate constant, transfer coefficient, respectively) as shown in Scheme 1.

A seen later on, the interference of reaction (2′) may be neglected. In other words, the "ECE" pathway (0 + 1 + 2) prevails over the disproportionation pathway (0 + 1 + 2′).[11a,e]

If the "ECE" reaction were to be controlled by the cleavage step (1), with reaction (0) acting as a pre-equilibrium, $\partial E_p/\partial \log v$ would be equal to 29.1 mV at 20 °C and to 23.3 mV at - 38 °C, while $E_{p/2} - E_p$ would be equal to 46.9 mV at 20 °C and to 37.6 mV at - 38 °C.[11]

Conversely, if the reaction were to be controlled by the electron transfer step, for a transfer coefficient equal to 0.5, $\partial E_p/\partial \log v$ would be equal to 58.2 mV at 20 °C and to 46.7 mV at −38 °C while $E_{p/2} - E_p$ would be equal to 93.8 mV at 20 °C and to 75.2 mV at −38 °C.[11] Both in DMF and in liquid NH_3, the value of these parameters lie in between the limiting values with, as expected, a clear tendency of passing from cleavage to electron transfer control upon raising the scan rate.[11] The competition between cleavage and electron transfer depends on a dimensionless parameter p which is defined by the following eq when $\alpha = 0.5$.

Scheme 2

$$P + e^- \rightleftharpoons Q$$

$$ArCH_2F + Q \underset{k_{-0}}{\overset{k_0}{\rightleftharpoons}} ArCH_2F^{\bullet -} + P \qquad (0')$$

$$ArCH_2F^{\bullet -} \xrightarrow{k_{1'}} ArCH_2^{\bullet} + F^- \qquad (1)$$

$$ArCH_2^{\bullet} + Q \rightleftharpoons ArCH_2^- + P \qquad (2')$$

$$p = \sqrt{\frac{2RT}{Fv}}\,\frac{k_S^{\,2}}{\sqrt{kD}}$$

From the theoretical variations of the peak potential and of the peak width with the parameter p,[11b] one may fit the experimental data in DMF (taking $D = 10^{-5}$ cm^2 s^{-1}) and in liquid NH_3 (taking $D = 3 \times 10^{-5}$ cm^2 s^{-1}) with $k_S^2/k^{1/2} = 1.8 \times 10^{-5}$ cm^2 s$^{-2.5}$ in the first case and $k_S^2/k^{1/2} = 2.4 \times 10^{-5}$ cm^2 s$^{-2.5}$ in the second. These fittings also provide the value of $E^0_{1'} + (RT/2F)\ln k$, −1.82 V vs SCE for DMF and −1.365 V vs 0.01 M Ag^+/Ag for liquid NH_3. Thus, if $E^0_{1'}$ or $k_{1'}$ could be known independently, the above relationships would provide the values of all three constants, $E^0_{1'}$, $k_{1'}$, and $k_{S,1'}$. We recourse to redox catalysis to obtain the lacking information.[11c] The reduction is observed indirectly by means of a reversible couple, P/Q, with a standard potential less negative than the reduction potential of the compound under investigation (Scheme 2). The variations of the catalytic increase of the current, i_p/i_p^0, upon addition of **1′** to a solution of P (i_p and i_p^0 are the peak currents in the presence and absence of the substrate, respectively) with concentrations and scan rate provide the desired information.

As seen from Scheme 2, there are two limiting kinetic regimes in the control of the catalytic response. If $k_{1'} \gg k_{-0}$[P], the catalytic current is governed by forward reaction (0′). Working curves relating i_p/i_p^0 to $(RT/F)(k_0[P]/v)$ for each value of the excess parameter, [substrate]/[P], are available,[11a,c] allowing the derivation of k_0 from the experimental data (see in Supporting Information how the rate constant was derided from the i_p/i_p^0 data). Conversely, when $k_{1'} \ll k_{-0}$[P], the catalytic current is governed by reaction (1), reaction (0′) then acting as a pre-equilibrium. Working curves relating i_p/i_p^0 to (RT/F) $(k_0k_{1'}/k_{-0}v)$ for each value of the excess parameter, [substrate]/[P], are available,[11a,c] allowing the derivation of $k_0k_{1'}/k_{-0}$ from the experimental data.

In DMF, with all four mediators indicated in Figure 3, the catalytic process is under the control of forward reaction 0′ as soon as [P] < 2.5 mM. The variation of log k_0 with, the standard potential of the mediator couple is close to 1/58.2 (mV^{-1}) indicating that the reverse reaction is under diffusion control reaction is under diffusion control. A procedure for determining the standard potential $E^0_{1'}$ ensues as depicted in Figure 3a. From the value thus found, −2.02 V vs SCE, one thus obtains, by use of the preceding peak potential and peak width data, $k_{1'} = 7 \times 10^6$ s^{-1} and $k_{S,1'} = 0.2$ cm s^{-1}.

In liquid NH_3, with a mediator such as 4-cyanopyridine, the variations of i_p/i_p^0 with the mediator concentration (see Supporting Information) indicate that there is mixed kinetic control

(11) (a) Andrieux, C. P.; Savéant, J.-M. Electrochemical Reactions. In *Investigations of rates and Mechanisms of Reactions*; Bernasconi, C. F., Ed.; Wiley: New York, 1986; Vol. 6, 4/E, Part 2, pp 305−390. (b) Nadjo, L.; Savéant, J.-M. *J. Electroanal. Chem.* **1973**, *48*, 113. (c) Andrieux, C. P.; Hapiot, P.; Savéant, J.-M. *Chem. Rev.* **1990**, *90*, 723. (d) Amatore, C.; Combellas, C.; Oturan, M. A.; Pinson, J.; Robvieille, S.; Savéant, J.-M.; Thiébault, A. *J. Am. Chem. Soc.* **1985**, *107*, 4846. (e) Amatore, C.; Savéant, J.-M. *J. Electroanal. Chem.* **1977**, *85*, 27.

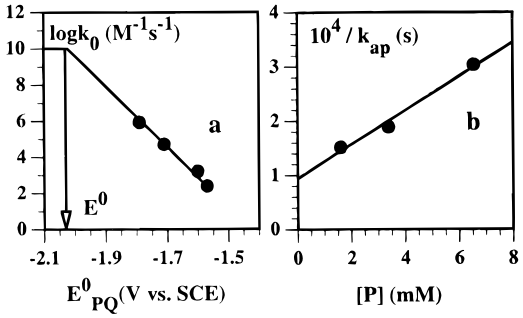

Figure 3. Redox catalyzed reduction of **1′** in DMF at 20°C (a) and in liq NH_3 at −38 °C (b). In a, the mediators are, from left to right, phthalonitrile (scan rates from 0.1 to 0.5 V/s), perylene (scan rates from 0.2 to 2 V/s), 4-cyanopryridine (scan rates from 2 to 20 V/s), 1-naphthonitrile (scan rates from 5 to 50 V/s), excess factor: from 0.5 to 5.3, mediator concentration: from 2 to 4.3 mM. In b, the mediator is 4-cyanopryridine, excess factor: from 0.7 to 4.3, mediator concentration: from 2 to 4.3 mM, scan rates from 0.1 to 1 V/s.

by reactions (0′) and (1). The value of the apparent rate constant k_{ap} defined as

$$\frac{1}{k_{ap}} = \frac{1}{k_0} + 0.33\frac{k_{-0}}{k_0 k_{1'}}[P] \qquad [1]$$

can be derived from the forced treatment of the i_p/i_p^0 data by the working curves corresponding to pure kinetic control by forward reaction (0).[11d] It is indeed found that the values of $1/k_{ap}$ thus determined vary linearly with the mediator concentration (Figure 3b). The validity of such an approximation rests on the fact that the shapes of the working curves for both limiting controls are almost the same. Replacing k_0 by $3k_0k_{1'}/k_{-0}$ in the first of these working curves gives a curve which is practically identical to the second working curve. The intercept of the linear plot (Figure 3b) provides k_0. Assuming that reverse reaction (0′) is under diffusion control thus leads to $E^0_{1'} = -1.54$ V vs 0.01 M Ag^+/Ag. The slope of the linear plot finally leads to $k_{1'} = 2.2 \times 10^7$ s^{-1}. Thus, the derivation of $E^0_{1'}$ and $k_{1'}$, i.e., the parameters of main interest, does not require the use of the peak potential and peak width data. It is however interesting to check that the values thus obtained are consistent with the value of $E^0_{1'} + (RT/2F)$ ln k (−1.365 V vs 0.01 M Ag^+/Ag) derived from these data. This is indeed the case since the value of the same potential found from the redox catalysis data is −1.369 V vs 0.01 M Ag^+/Ag. The value of $k_{S,1'}$ can then be obtained, $k_{S,1'} = 0.34$ cm s^{-1}.

As a test of consistency, the voltammograms obtained at 0.2 V/s, in the presence of an acid (Figure 1), have been simulated using the values of the various parameters that we just derived. As seen in Figure 1, the agreement between simulation and experiment is excellent. It should be however emphasized that redox catalysis experiments and systematic determination of the variation of the peak potential and peak width with the scan rate were necessary to obtain the exact values of $E^0_{1'}$, $k_{1'}$, and $k_{S,1'}$. The assumption, made at the start of this kinetic analysis that an "ECE" process is followed rather than a "DISP" process may be justified as follows. The parameter governing the competition between the two pathways is $(k_2'/k_{1'}^{3/2})$ [**1′**] $(Fv/RT)^{1/2}$,[11a,e] where $k_{2'}$ is close to the diffusion limit, 5×10^9 M^{-1} s^{-1} in DMF and 3×10^{10} M^{-1} s^{-1} in liquid NH_3. The value of the parameter ranges from 9.7×10^{-4} to 1.4×10^{-2} in DMF and 1.9×10^{-3} to 2.8×10^{-2} in liquid NH_3 when the scan rate varies from 0.2 to 2 V/s as in the experiments shown in Figure 2 indeed pointing to a large predominance of the ECE pathway.

Compound 1″. The reduction of **1″** also leads to the formation of 4-cyanotoluene, both in liquid NH_3 and in DMF,

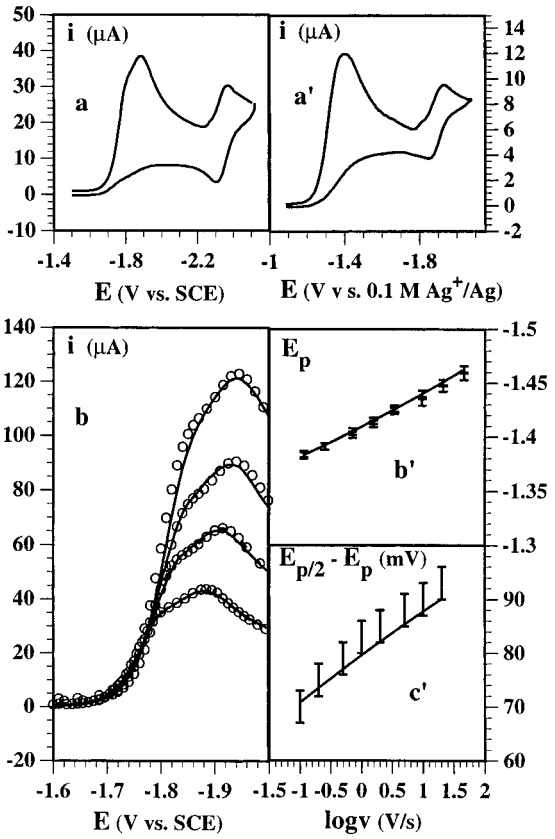

Figure 4. Reduction of 1 mM **1″** in DMF + 0.1 M n-Bu_4BF_4 at 20 °C (a) in the absence and (b) presence of acid (10 mM PhOH). Scan rate: (a) 0.2 V/s and (b) from bottom to top: 0.2, 0.5, 1, 2, V/s. Full lines: experimental curves, open circles: simulation according to Scheme 3. Reduction of 3 mM **1″** in liquid NH_3 + 0.1 M KBr + 3 mM NH_4^+ at −38°C at 0.2 V/s (a′). Variations of the peak potential (b′) and peak with (c′) with the scan rate.

as attested by the reversible one-electron wave following the first wave (Figures 4a,a′). In DMF, the addition of an acid such as phenol triggers a modest but distinct increase of the first wave, while the second wave becomes irreversible and increases up to a two-electron stoichiometry. In liquid NH_3, the presence of an equimolar amount of NH_4^+ leaves the second wave, which corresponds to the reduction of 4-cyanotoluene formed at the first wave, reversible as in the case of **1′**. In DMF, the first wave exhibits, at all investigated scan rates (0.1−10 V/s), a shoulder at potential *ca.* 70 mV more positive than the peak which is itself located at a potential very slightly more positive (*ca.* 30 mV) than the peak of **1′** (Figures 4a, b). Under these conditions, the peak height is not a straightforward indication of the electron stoichiometry. This is however clearly above 2 by comparison to the height of the one-electron reversible wave of 4-cyanotoluene. These observations points to the intermediacy of **1′** in the reductive cleavage of **1″** and thus to the reaction mechanism depicted in Scheme 3. In liquid NH_3, there is no splitting of the first wave. However, the electron stoichiometry is also clearly above 2 and the peak width is large (Figure 4a′,c′) pointing to the intermediacy of **1′** in the reductive cleavage of **1″** in this case too. We may thus assume that the reaction mechanism still follows Scheme 3.

Additional information may be derived from redox catalysis experiments. Using the same mediators as already used with **1′**, with the same scan rates, we found that the catalytic efficiency is larger than the maximal efficiency predicted for a two-electron stoichiometry of the reductive cleavage of **1″** by the reduced form of the mediator. Taking account of the fact

Scheme 3

$$\mathrm{ArCHF_2} + e^- \underset{}{\overset{E^0_{\mathbf{1}''},\, k_{S,\mathbf{1}''},\, \alpha_{\mathbf{1}''}}{\rightleftharpoons}} \mathrm{ArCHF_2^{\bullet -}} \qquad (0)$$

$$\mathrm{ArCHF_2^{\bullet -}} \xrightarrow{k_{\mathbf{1}''}} \mathrm{ArCHF^{\bullet}} + F^- \qquad (1)$$

$$(2)\quad \mathrm{ArCHF^{\bullet}} + e^- \rightleftharpoons \mathrm{ArCHF^-} \quad \text{and/or} \quad \mathrm{ArCHF^{\bullet}} + \mathrm{ArCHF_2^{\bullet -}} \longrightarrow \mathrm{ArCHF^-} + \mathrm{ArCHF_2} \qquad (2')$$

$$\mathrm{ArCHF^-} + H^+ \longrightarrow \mathrm{ArCH_2F} \qquad (3)$$

$$(4)\quad \mathrm{ArCH_2F} + e^- \overset{E^0_{\mathbf{1}'},\, k_{S,\mathbf{1}'},\, \alpha_{\mathbf{1}'}}{\rightleftharpoons} \mathrm{ArCH_2F^{\bullet -}} \quad \text{and/or} \quad \mathrm{ArCH_2F} + \mathrm{ArCHF_2^{\bullet -}} \rightleftharpoons \mathrm{ArCH_2F^{\bullet -}} + \mathrm{ArCHF_2} \qquad (4')$$

$$\mathrm{ArCH_2F^{\bullet -}} \xrightarrow{k_{\mathbf{1}'}} \mathrm{ArCH_2^{\bullet}} + F^- \qquad (5)$$

$$(6)\quad \mathrm{ArCH_2^{\bullet}} + e^- \rightleftharpoons \mathrm{ArCH_2^-} \quad \text{and/or} \quad \mathrm{ArCH_2^{\bullet}} + \mathrm{ArCHF_2^{\bullet -}} \longrightarrow \mathrm{ArCH_2^-} + \mathrm{ArCHF_2} \qquad (6')$$

$$\mathrm{ArCH_2^-} + H^+ \longrightarrow \mathrm{ArCH_3} \qquad (7)$$

Scheme 4

$$P + e^- \rightleftharpoons Q$$

$$\mathrm{ArCHF_2} + Q \underset{k_{-0,\mathbf{1}''}}{\overset{k_{0,\mathbf{1}''}}{\rightleftharpoons}} \mathrm{ArCHF_2^{\bullet -}} + P \qquad (0')$$

$$\mathrm{ArCHF_2^{\bullet -}} \xrightarrow{k_{\mathbf{1}''}} \mathrm{ArCHF^{\bullet}} + F^- \qquad (1)$$

$$\mathrm{ArCHF^{\bullet}} + Q \rightleftharpoons \mathrm{ArCHF^-} + P \qquad (2')$$

$$\mathrm{ArCHF^-} + H^+ \longrightarrow \mathrm{ArCH_2F} \qquad (3)$$

$$\mathrm{ArCH_2F} + Q \underset{k_{-0,\mathbf{1}'}}{\overset{k_{0,\mathbf{1}'}}{\rightleftharpoons}} \mathrm{ArCH_2F^{\bullet -}} + P \qquad (4')$$

$$\mathrm{ArCH_2F^{\bullet -}} \xrightarrow{k_{\mathbf{1}'}} \mathrm{ArCH_2^{\bullet}} + F^- \qquad (5)$$

$$\mathrm{ArCH_2^{\bullet}} + Q \rightleftharpoons \mathrm{ArCH_2^-} + P \qquad (6')$$

that the reduction of **1″** takes place at a potential more positive than the reduction potential of **1′**, this observation confirms the intermediacy of **1′** in the reductive cleavage of **1″** thus pointing to the catalytic mechanism depicted in Scheme 4. In order to obtain information pertaining solely to the reduction of **1″**, we used scan rates large enough for the catalytic response of **1′** to be negligible as anticipated from the experiments previously performed with **1′** alone. In DMF, it was found that the catalytic response obtained under these conditions, with the three mediators, 4-cyanopyridine ($E^0_{PQ} = -1.71$ V vs SCE), phthalonitrile ($E^0_{PQ} = -1.57$ V vs SCE), and quinoxaline ($E^0_{PQ} = -1.525$ V vs SCE), is governed by reaction 1 with 0′ acting as a pre-equilibrium (Scheme 4), provided [P] > 2 mM (see Supporting Information). The value of $(k_{0,\mathbf{1}''}/k_{-0,\mathbf{1}''})k_{\mathbf{1}''}$ could thus be derived with each catalyst (excess factor ranging from 0.7 to 4.1, mediator concentration ranging from 2 to 5.5 M). Since

$$\frac{RT}{F}\ln\left(\frac{k_{0,\mathbf{1}''}}{k_{-0,\mathbf{1}''}}k_{\mathbf{1}''}\right) = E^0_{\mathbf{1}''} - E^0_{PQ} + \frac{RT}{F}\ln(k_{\mathbf{1}''})$$

it was found that

$$E^0_{\mathbf{1}''} + \frac{RT}{F}\ln(k_{\mathbf{1}''})$$

$= -1.53$ V vs SCE in average.

We may thus combine this relationship with the shape and location of the cyclic voltammograms at various scan rates to derive the values of $E^0_{\mathbf{1}''}$, $k_{\mathbf{1}''}$, and of the heterogeneous electron transfer rate constant, $k_{S,\mathbf{1}''}$. The voltammograms simulated according to this procedure in the framework of Scheme 3 are shown together with the experimental curves in Figure 4b. It was thus found that $E^0_{\mathbf{1}''} = -1.89$ V vs SCE, $k_{\mathbf{1}''} = 2 \times 10^5$ s^{-1}, $k_{S,\mathbf{1}''} = 0.35$ cm s^{-1}. It is worth noting that the results of the simulations do not change appreciably when the homogeneous electron transfer steps (2′), (4′), and (6′), where the electron donor is the anion radical of **1″**, are not included in the simulation. This observation points to the conclusion that electron transfer to ArCHF•, $ArCH_2F$, and $ArCH_2$• takes place predominantly at the electrode surface according to reactions (2), (4), and (5). In other words the various follow-up electron transfer steps take place according to an "ECE" process rather than to a "DISP" process.[11a,e] The parameter governing the competition between the two pathways is $(k_2'/k_{\mathbf{1}''}^{3/2})[\mathbf{1}''](Fv/RT)^{1/2}$ where k_2' is close to the diffusion limit, 5×10^9 M^{-1} s^{-1}. The value of the parameter in the present case ranges from 0.15 to 0.5 when the scan rate varies from 0.2 to 2 V/s as in the experiments shown in Figure 4b indeed pointing to the predominance of the ECE pathway. In other words, the homogeneous "internal" redox catalysis of the reduction of **1′** by the anion radical of **1″** is inefficient in the present case because of its instability toward fluoride cleavage.

The data for liquid NH_3 (see Supporting Information) were treated in the same way as for DMF. Using 4-cyanopyridine as a mediator, it was again found that, provided [P] > 2 mM, the catalytic response is governed by reaction (1) with (0′) acting as a pre-equilibrium. Over the whole range of excess factors (0.5−3.3), mediator concentrations (2−5.8 mM), and scan rates (2−10 V/s), it was found that $(k_{0,\mathbf{1}''}/k_{-0,\mathbf{1}''})k_{\mathbf{1}''} = 37$ s^{-1}, and thus, since $E^0_{PQ} = -1.25$ V vs 0.01 M Ag^+/Ag, $E^0_{\mathbf{1}''} + RT/F\ln(k_{\mathbf{1}''}) = -1.18$ V vs 0.01 M Ag^+/Ag. The simulation of the cyclic voltammetric responses, using this relationship, are shown in Figures 4b′,c′, as variations of the peak potential and peak width with the scan rate. We thus obtained $E^0_{\mathbf{1}''} = -1.45$ V vs 0.01 M Ag^+/Ag, $k_{\mathbf{1}''} = 1 \times 10^6$ s^{-1}, $k_{S,\mathbf{1}''} = 0.6$ cm s^{-1}.

Compound 1‴. The preceding results indicate that the anion radical cleavage rate constant decreases from **1′** to **1″**. We may thus expect a further decrease when going to **1‴**. We indeed observed, both in DMF and in liquid NH_3, that the reduction wave of **1‴** becomes reversible upon raising the scan rate (Figure 5), thus offering a new strategy for determining the

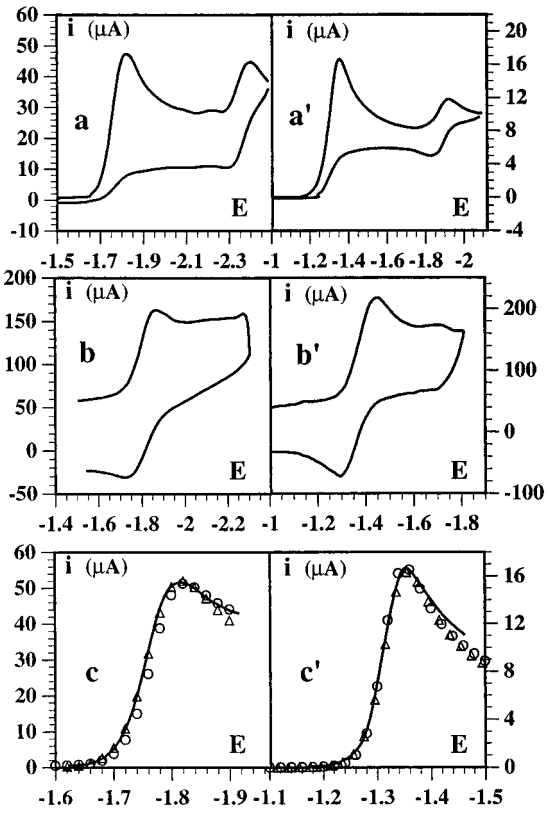

Figure 5. Reduction of **1‴** in DMF + 0.1 M *n*-Bu_4BF_4 at 20 °C (a, b) + 10 mM PhOH (c), and in liquid NH_3 + 0.1 M KBr + 3 mM NH_4Br] at −38 °C (a′, b′, c′). [**1‴**] = 1 mM (a, b, c), 3 mM (a′, b′, c′). Scan rate: 0.2 (a, a′, c, c′), 50 (b), and 300 (b′) V/s. The potentials are referred to SCE in DMF and to 0.01 M Ag^+/Ag in liquid NH_3. Solid lines: experimental data. Open circles: simulation according to Scheme 5. Open triangles: simulation according to the "internal" redox catalysis mechanism.

mechanism and characteristics of the reductive cleavage of this compound. At low scan rates, the first wave, which is then irreversible, corresponds to the exchange of *ca.* six electrons per molecule, pointing to the mechanism depicted in Scheme 5.

Once the standard potential $E^0_{\mathbf{1}'''}$ has been determined as the midpoint between the cathodic and anodic peak of the one-electron reversible wave obtained upon raising the scan rate, the value of $k_{\mathbf{1}'''}$ and $k_{S,\mathbf{1}'''}$ can be derived from the simulation of the irreversible cyclic voltammograms obtained at low scan rates according to Scheme 5, taking into account the previously derived values of $E^0_{\mathbf{1}''}$, $k_{\mathbf{1}''}$, $k_{S,\mathbf{1}''}$ and of $E^0_{\mathbf{1}'}$, $k_{\mathbf{1}'}$, $k_{S,\mathbf{1}'}$.

Examples of the fit between simulations and experiments are shown in Figure 5c,c′. We thus found $E^0_{\mathbf{1}'''} = -1.785$ V vs SCE, $k_{\mathbf{1}'''} = 38$ s^{-1}, $k_{S,\mathbf{1}'''} = 0.1$ cm s^{-1} in DMF and $E^0_{\mathbf{1}'''} = -1.345$ V vs 0.01 M Ag^+/Ag, $k_{\mathbf{1}'''} = 350$ s^{-1}, $k_{S,\mathbf{1}'''} = 0.25$ cm s^{-1} in liquid NH_3.

Since the cleavage rate constants are small in both media, we expect the homogeneous electron transfer steps (2′), (4′), (6′), (8′), and (10′) to prevail over their heterogeneous counterparts. The parameter $(k_{2'}/k_{\mathbf{1}'''}{}^{3/2})$ $[\mathbf{1}'''](Fv/RT)^{1/2}$ is indeed equal to 1.2×10^5 in DMF and to 4.3×10^4 in liquid NH_3 in the experiments shown in Figure 5 (parts c and 5c′ respectively). Accordingly, simulation taking only into account the homogeneous electron transfer steps produces curves that were found to be in good agreement with the experimental curves as well as with the theoretical curves involving the complete set of reactions in Scheme 5. "Internal" redox catalysis of the reduction of **1″** and **1′** by the anion radical of **1‴** thus completely overcomes their direct reduction at the electrode.

Table 1. Standard Potentials and Cleavage Rate Constants of 4-Cyanofluorotoluenes

	medium			
	DMF at 20 °C		liquid NH_3 at −38 °C	
compd	$E^{0\,a}$	$k_{cleav}{}^c$	$E^{0\,b}$	$k_{cleav}{}^c$
1′	−2.020	7×10^6	−1.540	2.2×10^7
1″	−1.890	4×10^5	−1.450	1×10^6
1‴	−1.785	3.8×10^1	−1.345	3.5×10^2

[a] V vs SCE. [b] V vs 0.01 M Ag^+/Ag. [c] In s^{-1}.

Table 2. Standard Potentials and Cleavage Rate Constants of the Trifluoromethylarenes in Liquid NH_3 at −38 °C

compd	$E^{0\,a}$	$k_{cleav}{}^b$	compd	$E^{0\,a}$	$k_{cleav}{}^b$
1‴	−1.345	3.5×10^2	**6**	−1.835	1.1×10^4
2	−1.480	1×10^1	**7**	−2. 180	2.8×10^8
3	−1.385	1.5×10^2	**8**	−1.650	2×10^7
4	−1.330	7.5	**9**	−2.075	1×10^7
5	−1.405	2.5×10^1			

[a] V vs 0.01 M Ag^+/Ag. [b] In s^{-1}.

The standard potentials and cleavage rate constants for **1′**, **1″**, and **1‴** are listed in Table 1.

Other Compounds. We now describe the cyclic voltammetric behavior of the other trifluoro-compounds (see Chart 1), for which the corresponding difluoro- and monofluoro-compounds were not available, with the aim of determining the standard potential for the formation of the anion radical and its cleavage rate constant in liquid ammonia. Among them, compounds **2**−**5** resemble compound **1‴**. At low scan rate, they likewise exhibit a large irreversible wave, with a stoichiometry corresponding to six electrons per molecule, followed by a reversible one-electron wave corresponding to the $ArCH_3$ compound formed at the first wave upon reductive cleavage of the three fluorine atoms (Figure 6). Also, like with **1‴**, the cleavage rate constant is not very large, and thus, reversibility does not require a very high scan rate to be reached (Figure 6). The ensuing values of the standard potential are listed in Table 2. We thus expect the reductive cleavage of these four compounds to take place according to the internal redox catalysis mechanism. That this is indeed the case results from the good fit of the curves simulated according to this mechanism with the experimental curves (Figure 6), thus leading to the values of the cleavage rate constant listed in Table 2. With **4**, the second wave is large, poorly defined and irreversible unlike the second wave of **1‴**, **2**, **3**, and **5**. It nevertheless corresponds to the reduction of the 4-carboxymethyl toluene as checked with an authentic sample of the latter compound. The reason for this particular behavior of the 4-carboxymethyl toluene in liquid ammonia (in DMF it gives rise to a one-electron reversible wave) is not known for the time being. We may finally estimate the value of the parameter that governs the competition between the internal redox catalysis mechanism and the ECE mechanism, $(k_{2'}/k_{\mathbf{1}'''}{}^{3/2})[\mathbf{1}''](Fv/RT)^{1/2}$, for **2**, **3, 4**, and **5**, 9×10^6, 2×10^5, 10^7, 7×10^4, respectively, thus showing that the former mechanism largely overruns the latter in all four cases.

The cyclic voltammetry of **6** has in common with that of **1‴** and **2**−**5** that it exhibits an irreversible wave with a *ca.* six-electron stoichiometry at low scan rate (Figure 7). There are however two important differences. One is that there is no second wave corresponding to the reduction of the defluorinated product formed at the first wave. The lack of a second wave is due to the fact that the 4-methyl-benzoate anion does not exhibit, because of the negative charge it bears, any reduction wave prior the discharge of the supporting electrolyte. The second difference is that the 6e-wave remains irreversible over the available

Scheme 5[a]

$$\overset{E^0_{1'''},\ k_{S,1'''},\ \alpha_{1'''}}{ArCF_3 + e^- \rightleftharpoons ArCF_3^{\bullet -}} \qquad (0)$$

$$ArCF_3^{\bullet -} \xrightarrow{k_{1'''}} ArCF_2^{\bullet} + F^- \qquad (1)$$

$$(2)\quad ArCF_2^{\bullet} + e^- \rightleftharpoons ArCF_2^- \quad \text{and/or} \quad ArCF_2^{\bullet} + ArCF_3^{\bullet -} \longrightarrow ArCF_2^- + ArCF_3 \qquad (2')$$

$$ArCF_2^- + H^+ \longrightarrow ArCHF_2 \qquad (3)$$

$$\overset{E^0_{1''},\ k_{S,1''},\ \alpha_{1''}}{(4)\quad ArCHF_2 + e^- \rightleftharpoons ArCHF_2^{\bullet -}} \quad \text{and/or} \quad ArCHF_2 + ArCF_3^{\bullet -} \rightleftharpoons ArCHF_2^{\bullet -} + ArCF_3 \qquad (4')$$

$$ArCHF_2^{\bullet -} \xrightarrow{k_{1''}} ArCHF^{\bullet} + F^- \qquad (5)$$

$$(6)\quad ArCHF^{\bullet} + e^- \rightleftharpoons ArCHF^- \quad \text{and/or} \quad ArCHF^{\bullet} + ArCF_3^{\bullet -} \longrightarrow ArCHF^- + ArCF_3 \qquad (6')$$

$$ArCHF^- + H^+ \longrightarrow ArCH_2F \qquad (7)$$

$$\overset{E^0_{1'},\ k_{S,1'},\ \alpha_{1'}}{(8)\quad ArCH_2F + e^- \rightleftharpoons ArCH_2F^{\bullet -}} \quad \text{and/or} \quad ArCH_2F + ArCF_3^{\bullet -} \rightleftharpoons ArCH_2F^{\bullet -} + ArCF_3 \qquad (8')$$

$$ArCH_2F^{\bullet -} \xrightarrow{k_{1'}} ArCH_2^{\bullet} + F^- \qquad (9)$$

$$(10)\quad ArCH_2^{\bullet} + e^- \rightleftharpoons ArCH_2^- \quad \text{and/or} \quad ArCH_2^{\bullet} + ArCF_3^{\bullet -} \longrightarrow ArCH_2^- + ArCF_3 \qquad (10')$$

$$ArCH_2^- + H^+ \longrightarrow ArCH_3 \qquad (11)$$

[a] The homogeneous electron transfer steps are assumed to involve only the anion radical of $ArCF_3$ as electron donor ((2′), (4′), (6′), (8′), (10′)) and not the anion radical of $ArCHF_2$ and anion radical of ArCH2F in accordance with the fact that the latter species cleave much more rapidly than the former.

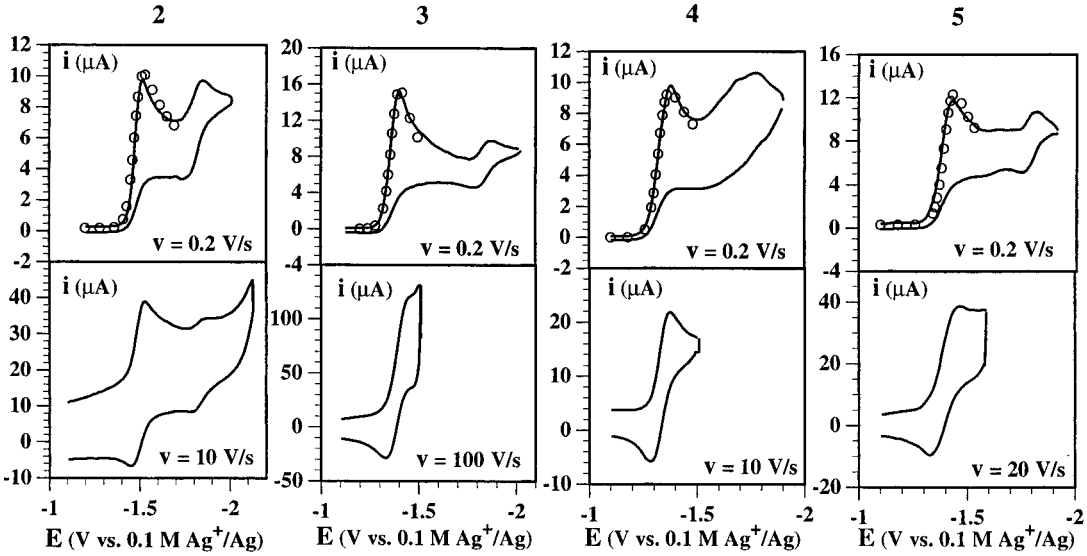

Figure 6. Cyclic voltammetry of **2**, **3**, **4**, and **5** (3 mM) in liquid NH_3 + 0.1 M KBr + 3 mM NH_4Br] at −38 °C. Open circles: simulation according to the "internal" redox catalysis mechanism.

range of scan rates (0.2−200 V/s) indicating that the cleavage of the anion radical of $ArCF_3$ is faster. It follows that the standard potential cannot be derived from cyclic voltammetric experiments, thus preventing the application of the procedure used with **1‴** and **2**−**5**. The lacking piece of information can however be obtained from redox catalysis as described below.

8 and **9** also give rise (Figure 7) to a single wave which remains irreversible over the available range of scan rates. As with **6**, the totally defluorinated products do not exhibit reduction waves within the available potential range. There is however an important difference with **6**, namely that the reduction wave is a composite wave pointing to an ECE mechanism in which the di- and monofluoro products formed from the initial trifluoro compound are successively reduced at the electrode surface. In these two cases the instability of the primary anion radical prevents the internal redox catalysis mechanism to compete with the ECE mechanism. With **6**, the reduction wave does not show any splitting leading to the conclusion that the internal redox catalysis mechanism overruns the ECE mechanism in this case. We will see, once the cleavage rate constants will be determined, that the cleavage of the anion radical of **6**, albeit faster than with **1‴** and **2**−**5**, is indeed slower than with **8** and **9** thus giving

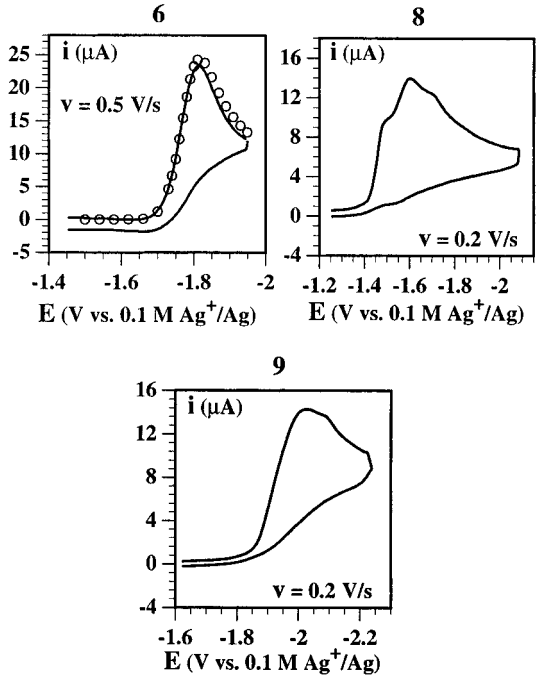

Figure 7. Cyclic voltammetry of **6**, **8**, and **9** (3 mM) in liquid NH_3 + 0.1 M KBr at −38 °C. Open circles: simulation according to the "internal" redox catalysis mechanism.

more chance to the internal redox catalysis mechanism to compete with the ECE mechanism. We may thus simulate the low scan rate cyclic voltammograms of **6** according to the internal redox catalysis mechanism. However, since the standard potential could not be derived from cyclic voltammetry, we need additional information to derive the values of the standard potential and of the cleavage rate constant. This can be obtained from redox catalysis. As a mediator we used pyridazine. Because its standard potential (−1.565 V vs 0.01 M Ag^+/Ag) is rather positive, the catalytic increase of the current is rather modest. Under these conditions, the scan rate could be adjusted so as to render negligible the interference of electron transfer from the reduced form of the catalyst, Q, to the difluoro and monofluoro products, thus attempting to use the same strategy that was successfully employed in the case of **1″**. However, even if Q is unable to reduce the difluoro and monofluoro products, the anion radical of **6**, produced by reaction with Q, may well reduce these products as we know from the observation that the direct reduction of **6** occurs predominantly through the internal redox catalysis mechanism. We are thus led to treat the redox catalysis data in the framework of the mechanism depicted in Scheme 6. It was found that the catalytic increase of the current is independent of the catalyst concentration showing that the kinetics are governed by the factor $k\,k_0/k_{-0}$. Its value, derived from the appropriate working curves,[12] is 0.0017. $(RT/F)\ln(k\,k_0/k_{-0}) = E^0 - E^0_{PQ} + (RT/F)\ln k$. Thus $E^0 + (RT/F)\ln k = -1.647$ V vs 0.01 M Ag^+/Ag. Potentially, the cyclic voltammogram of **6** (Figure 7) contains two relationships between E^0, k, and k_S. Simulation of the voltammogram in Figure 7 according to the internal redox catalysis mechanism, taking into account the relationship

(12) (a) The working curves for a given excess factor, [$ArCH_3$]/[P], are the same as the working curves pertaining to a simple EC mechanism for an excess factor of 6 [$ArCH_3$]/[P].[10a,11b] For **1″**, **7**, **8**, and **9**, the working curves for a given excess factor [$ArCH_3$]/[P] are the same as the working curves pertaining to a simple EC mechanism for an excess factor of 2 [$ArCH_3$]/[P],[10a,11b] for mediators giving rise to a small catalytic effect. (b) Andrieux, C. P.; Dumas-Bouchiat, J.-M.; Savéant, J.-M. *J. Electroanal. Chem.* **1978**, *87*, 55.

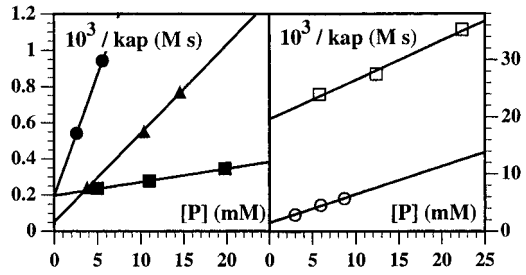

Figure 8. Figure 8. Redox catalysis of the reduction of compounds **7**, **8**, and **9** in liquid NH_3 + 0.1 M KBr at −38 °C. Variation of the apparent rate constant (eq [1]) with the mediator concentration.

point	compd	mediator	$-E^0_{PQ}$ [a]
■	7	benzonitrile	1.785
□		4-toluonitrile	1.870
●	8	dimethylquinoxaline	1.300
○		4,4′-bipyridine	1.330
▲	9	benzonitrile	1.785

[a] V vs 0.01 M Ag^+/Ag.

between E^0 and k derived from redox catalysis finally lead to $E^0 = -1.830$ V vs 0.01 M Ag^+/Ag, $k = 9 \times 10^3$ s^{-1}, $k_S = 0.1$ cm s^{-1}. This value of k is consistent with the fact that the redox catalysis is under the kinetic control of reaction 1 with 0′ acting as a pre-equilibrium. Indeed, $k_{-0}[P]/k = 10^4$ (k_{-0} is certainly close to the diffusion limit, 3×10^{10} M^{-1} s^{-1}). We may also estimate the value of the parameter that governs the competition between the internal redox catalysis mechanism and the ECE mechanism in the direct electrochemical reduction of **6**, $(k_{2'}/k_{1''}^{3/2})[\mathbf{1''}](Fv/RT)^{1/2}$. This is equal to 3×10^2, which confirms that the former mechanism largely predominates over the later.

Redox catalysis needed also to be used in the case of **8** and **9** for which k is expected to be even larger than with **6**. This is also the case with **7**, for which, in addition, self-inhibition heavily perturbs the cyclic voltammetric curves so as to render the extraction of kinetic information untractable. The variation of the catalytic responses (see Supporting Information) with the mediator concentration showed that catalysis is under mixed kinetic control by reactions (0′) and (1). We may therefore treat the data by means of eq [1] as summarized in Figure 8 leading to the values of E^0 and k listed in Table 1.

In the reductive cleavage of the di- and trifluoro derivatives, we did not consider so far another mechanistic possibility namely the intermediacy of carbenes. Such mechanisms would involve the replacement of reactions (3), (4), (4′), and (5) in Scheme 3 by reactions (3), (4), (4′), and (5) in Scheme 7. Formation of carbenes as intermediate in the electrochemical reduction of *gem*-dichloro, dibromo, and chlorobromo compounds has precedency.[8] The possibility of such a reaction with our di- and trifluoro derivatives should therefore be examined, even if it has never been reported so far. Reduction potentials of carbenes are not known. However, being electron-deficient species they may be easier to reduce (eqs [4] and [4′]) than the starting fluoro compound. The carbene anion radical thus formed would then be protonated (reaction (5)) giving rise to a radical which is easier to reduce than the starting fluoro compound yielding eventually the defluorinated product. If the carbene mechanism were to be followed, the monofluorinated derivative would not be an intermediate in the reductive cleavage of the difluoro compounds, and the difluorinated derivative would not be an intermediate in the reductive cleavage of the trifluoro compounds. The carbene mechanism may thus be ruled out in the case of **1″** since the reduction wave of **1′** appears in its cyclic voltammogram. It may likewise be ruled out in

Scheme 6

$$P + e^- \rightleftharpoons Q$$

$$ArCF_3 + Q \underset{k_{-0}}{\overset{k_0}{\rightleftharpoons}} ArCF_3^{\bullet -} + P \quad (0')$$

$$ArCF_3^{\bullet -} \xrightarrow{k} ArCF_2^{\bullet} + F^- \quad (1)$$

$$(2'')\ ArCF_2^{\bullet} + Q \longrightarrow ArCF_2^- + P \qquad ArCF_2^{\bullet} + ArCF_3^{\bullet -} \longrightarrow ArCF_2^- + ArCF_3 \quad (2')$$

$$ArCF_2^- + H^+ \longrightarrow ArCHF_2 \quad (3)$$

$$ArCHF_2 + ArCF_3^{\bullet -} \rightleftharpoons ArCHF_2^{\bullet -} + ArCF_3 \quad (4')$$

$$ArCHF_2^{\bullet -} \longrightarrow ArCHF^{\bullet} + F^- \quad (5)$$

$$(6'')\ ArCHF^{\bullet} + Q \longrightarrow ArCHF^- + P \qquad ArCHF^{\bullet} + ArCF_3^{\bullet -} \longrightarrow ArCHF^- + ArCF_3 \quad (6')$$

$$ArCHF^- + H^+ \longrightarrow ArCH_2F \quad (7)$$

$$ArCH_2F + ArCF_3^{\bullet -} \rightleftharpoons ArCH_2F^{\bullet -} + ArCF_3 \quad (8')$$

$$ArCH_2F^{\bullet -} \longrightarrow ArCH_2^{\bullet} + F^- \quad (9)$$

$$(10'')\ ArCH_2^{\bullet} + Q \longrightarrow ArCH_2^- + P \qquad ArCH_2^{\bullet} + ArCF_3^{\bullet -} \longrightarrow ArCH_2^- + ArCF_3 \quad (10')$$

$$ArCH_2^- + H^+ \longrightarrow ArCH_3 \quad (11)$$

Scheme 7

Difluoro compounds

$$ArCHF^- \longrightarrow Ar\ddot{C}H + F^- \quad (3)$$

$$(4)\quad Ar\ddot{C}H + e^- \rightleftharpoons Ar\dot{C}H^- \quad \text{and/or} \quad Ar\ddot{C}H + ArCHF_2^{\bullet -} \rightleftharpoons Ar\dot{C}H^- + ArCHF_2 \quad (4')$$

$$Ar\dot{C}H^- + H^+ \longrightarrow ArCH_2^{\bullet} + F^- \quad (5)$$

Trifluoro compounds

$$ArCF_2^- \longrightarrow Ar\ddot{C}F + F^- \quad (3)$$

$$(4)\quad Ar\ddot{C}F + e^- \rightleftharpoons Ar\dot{C}F^- \quad \text{and/or} \quad Ar\ddot{C}F + ArCF_3^{\bullet -} \rightleftharpoons Ar\dot{C}F^- + ArCF_3 \quad (4')$$

$$Ar\dot{C}F^- + H^+ \longrightarrow Ar\dot{C}HF \quad (5)$$

$$ArCHF^- \longrightarrow Ar\ddot{C}H + F^- \quad (7)$$

followed by the same reactions as reactions (4) (4') and (5) in the case of difluoro compounds

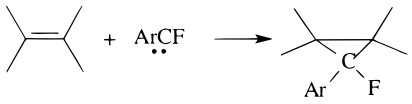

(8)

the case of **8** and **9** since both the difluoro and monofluoro compounds appear in their voltammograms. All other trifluoro compounds show a single 6e wave. Their reductive cleavage may go through the di- and monofluoro derivatives in the framework of the internal redox catalytic mechanism discussed earlier. However, it may also *a priori* follow the carbene mechanism. A first argument against the latter possibility is that there no obvious reasons that it would be followed with **1‴** and **2**−**6** and not with **1″**, **8**, and **9**.

We investigated the possible occurrence of the carbene mechanism in more details in the case of **1‴**. Phenylfluorocarbene has been previously obtained by deprotonation of α,α′-bromofluorotoluene. Because of its electrophilic character it reacts quantitatively with the electron rich olefin, 2,3-dimethyl-2-butene. Since 4-cyanophenylfluorocarbene should be even more electrophilic, we have selected the same olefin to attempt a trapping experiment (reaction 8 in Scheme 7). **1‴** was electrolyzed (see Experimental Section) in the presence of a large excess of 2,3-dimethyl-2-butene. The only product found was 4-toluonitrile. The lack of reaction may be explained by the observation that no reaction occurs when **1″** is deprotonated by *t*-BuO$^-$ in the presence of the same olefin (see Experimental Section), in exactly the same conditions as those of the experiment described above where quantitative carbene addition is observed with bromofluorotoluene as the substrate. We may thus conclude that the carbene does not form from the base of **1″** presumably because the C−F bond is much stronger than the C−Br bond. These observations confirm that the carbene mechanism is not followed in the reductive cleavage of the trifluoro compounds we have investigated.

Discussion

The mechanism of the reductive cleavage of the compounds investigated has been established in the preceding section. Besides its own interest, the knowledge of the mechanism was necessary to derive correct values of the standard potential and the cleavage rate constant of the primary anion radical. These are gathered in Tables 1 and 2.

We first discuss the reactivity−structure relationships for the reductive cleavage of the three 4-cyanofluorotoluenes. A first observation is that, in both solvents, the cleavage rate constant decreases when the number of fluorine increases. The intramolecular dissociative electron transfer model of anion radical cleavage[9] may be applied to explain this observation. The predictions of the model are contained in the following eqs

$$\frac{RT}{F}\ln k_{cleav} = \frac{RT}{F}\ln\frac{kT}{h} - \Delta G^{\ddagger} \qquad [2]$$

(in the following, energies are expressed in eV and potentials in V)

$$\Delta G^{\ddagger} = \Delta G_0^{\ddagger}\left(1 + \frac{\Delta G^0}{4\Delta G_0^{\ddagger}}\right)^2 \approx \Delta G_0^{\ddagger} + \frac{\Delta G^0}{2} \qquad [3]$$

The second, approximate, version of eq [3] is valid as long as the driving force of the reaction, $-\Delta G^0$, is small as compared to the total reorganization energy, $4\Delta G_0^{\ddagger}$. The driving force may be expressed by eq [4] as a function of the bond dissociation energy of the starting compound, D_{RX}, of the standard potential for the formation of the anion radical, $E^0_{RX/RX^{\bullet -}}$ and the standard potential for the oxidation of the leaving anion X^-, (the *s*'s are the molar entropies of the subscript species).

$$\Delta G^0 = D_{RX} + E^0_{RX/RX^{\bullet -}} - E^0_{X^{\bullet}/X^-} - T(s_{R^{\bullet}} + s_{X^{\bullet}} - s_{RX}) \quad [4]$$

The intrinsic barrier free energy, $\Delta G_0^{\ddagger}$ is the sum of two terms. One, $\Delta G^{\ddagger}_{0,intra}$, deals with the intramolecular nuclear rearrangement accompanying the cleavage of the C−X bond. It may be expressed by eq [5] as a function of the bond dissociation energy of the starting compound, D_{RX}, of the standard potential for the formation of the anion radical, $E^0_{RX/RX^{\bullet -}}$ and the standard potential for the oxidation of R^-

$$4\Delta G^{\ddagger}_{0,intra} = D_{RX^{\bullet -}} = D_{RX} + E^0_{RX/RX^{\bullet -}} - E^0_{R^{\bullet}/R^-} + T(s_{RX} - s_{RX^{\bullet -}} + s_{R^-} - s_{R^{\bullet}})$$

$$= D_{RX} + (h_{RX} - h_{RX^{\bullet -}}) - (h_{R^{\bullet}} - h_{R^-}) \qquad [5]$$

(the *h*'s are the molar enthalpies of the subscript species).

The other, $\Delta G^{\ddagger}_{0,solv}$, involves the solvent reorganization that arises from the displacement of the negative charge from the aromatic portion of the molecule to the leaving fluoride ion. $\Delta G^{\ddagger}_{0,solv}$ may thus be estimated from eq [6]

$$\Delta G^{\ddagger}_{0,solv} = \frac{e_0^2}{4}\left(\frac{1}{2a_{RX^{\bullet -}}} + \frac{1}{2a_{R^{\bullet},X^-}} - \frac{1}{d}\right)\left(\frac{1}{D_{op}} - \frac{1}{D_s}\right) \qquad [6]$$

e_0 is the electron charge, $a_{RX^{\bullet -}}$ is the radius of the sphere approximating the region of the starting anion radical where the charge is initially located, and $a_{R^{\bullet},X^-}$, the radius of the sphere approximating the location of the charge on the leaving group when the bond is broken. *d* is the distance between the centers of charge. The *D*'s are the optical and static dielectric constants, respectively.

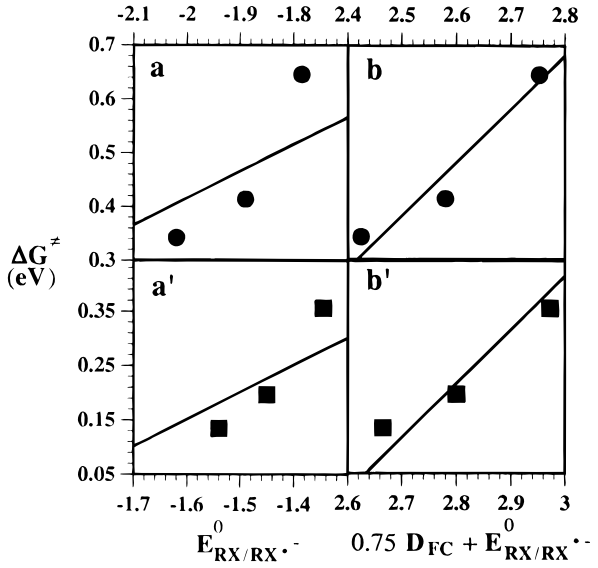

Figure 9. Correlation between the activation free energy of the anion radical cleavage of (from left to right) **1′**, **1″**, and **1‴** with the standard potential $E^0_{RX/RX^{\bullet}}$ (a, a′) and the function $0.75D_{FC} + 0.5E^0_{RX/RX^{\bullet}}$ (b, b′), in DMF at 20 °C (●) and liquid NH_3 at −38 °C (■).

The standard potential $E^0_{RX/RX^{\bullet -}}$ becomes more and more positive from **1′** to **1″** and **1‴** (Table 1) as a consequence of the increasing electron-withdrawing effect of the fluoromethyl group on the π^* orbital of the aromatic moiety. The driving force of the cleavage reaction decreases accordingly (eq [4]). This is a first reason why the cleavage rate constant decreases from **1′** to **1″** and **1‴**. If the C−F bond dissociation energy and the intrinsic barrier were to remain constant in the series, the linearized version of eqs [3] and [4] would imply that the activation free energy should vary linearly with the driving force with a slope of 0.5:

$$\Delta G^{\ddagger} = \frac{E^0_{RX/RX^{\bullet -}}}{2} + \text{Cst}$$

As seen in Figure 9a,a′, this prediction is not correct in both solvents. The experimental activation free energy varies more than predicted from the mere variation of the standard potential. There is evidence that the C−F bond dissociation energy varies with the number of fluorine atoms borne by the functional carbon. Quantitative data are available for *gem*-fluoroalkanes, e.g., for *gem*-fluoroethanes (4.58, 4.70, 4.86 eV for $-CH_2F$, $-CHF_2$, and $-CF_3$, respectively).[14] The bond dissociation energy interferes both in the driving force (eq [4]) and in the intrinsic barrier. Using the linearized version of eq [3], we may thus attempt a correlation of the experimental activation free energy with $0.75D_{FE} + 0.5E^0_{RX/RX^{\bullet -}}$ (where the D_{FE}'s are the bond dissociation energies of the *gem*-fluoroethanes). Such an attempt implies several assumptions: (i) the increments in the BDEs of **1′**, **1″**, **1‴** are the same as for the corresponding fluoroethanes; (ii) the entropic term in eq [4] is the same for the three compounds (it essentially corresponds to the formation of two particles out of one and should not therefore vary much in the series); and (iii) $(h_{RX} - h_{RX^{\bullet -}}) - (h_{R^{\bullet}} - h_{R^-} + \Delta G^{\ddagger}_{0,solv}$ is about constant. The first term increases from **1′** to **1‴** because of the increasing electron-withdrawing effect of the fluoromethyl group on the LUMO energy. The second term increases in a parallel fashion because the increasing electron-

(13) (a) Moss, R. A.; Przybyla, J. R. *Tetrahedron* **1969**, *25*, 647. (b) Moss, R. A. *Acc. Chem. Res.* **1980**, *13*, 58.

(14) Joshi, R. M. *J. Macromol. Sci.-Chem.* **1974**, *A8*, 861

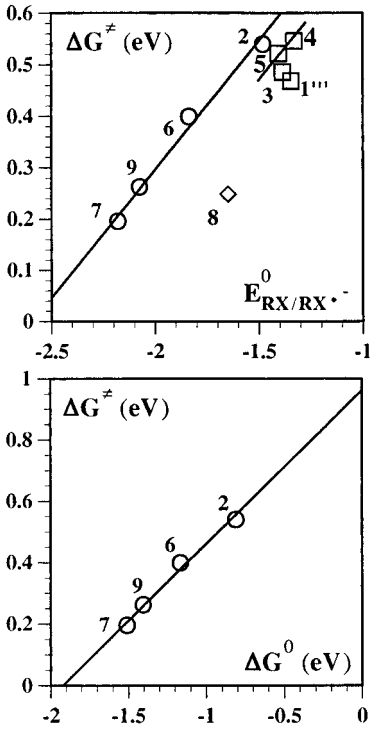

Figure 10. Cleavage of the anion radical of the trifluoromethylarenes in liquid NH_3 at −38 °C. Correlation between the activation free energy with the standard potential (in V vs 0.01 M Ag^+/Ag) (a) and the reaction standard free energy (b).

withdrawing effect of the fluoromethyl group renders the oxidation of the anion R- more and more difficult. It may thus be considered that the variation of the first term is compensated by the variation of the second. In the expression of $\Delta G^{\ddagger}_{0,solv}$, the most important factor in the first parenthesis is the second term because the radius of the fluoride anion is smaller than the radius pertaining to the anion radical and the center-to-center distance. The third term in $\Delta G^{\ddagger}_0$ may therefore be regarded as approximately constant. As seen in Figure 9b,b′, there is indeed a satisfactory linear correlation between the experimental activation free energy and $0.75D_{FE} + 0.5E^0_{RX/RX\cdot^-}$. A more quantitative analysis of the activation vs driving force relationship will be presented later on, after examination of the rate data pertaining to the trifluoro compounds in liquid NH_3 (Table 2). Another striking feature of the cleavage kinetics of the anion radicals of **1′**, **1″**, and **1‴**, is that the activation free energies are smaller in liquid NH_3 than in DMF (Figure 9) in spite of a 50 °C difference in temperature. As discussed later on, in more quantitative terms, this larger cleavage reactivity in liquid NH_3 derives essentially from the stabilization of F^- by NH_3 as compared to DMF, resulting in a driving force advantage (eq [4]) which is not compensated by the decrease in temperature. NH_3 is indeed a more protic solvent than DMF, hence leading to a H-bonding stabilization of anions such as F^-.

We now examine the rate data pertaining to the anion radical cleavage in the whole series of trifluoromethylarenes in liquid NH_3 at −38 °C (Table 2). Figure 10a shows that there is a rough correlation between the activation free energy and the standard potential for the formation of the anion radical (the more negative the later the smaller the former) as expected from the attending variation of the driving force (eq [4]). It is remarkable that the data points of **2**, **6**, **7**, and **9** sit on a single straight line with a slope of 0.5, indicating that the C−F bond dissociation energy is closely the same for these four compounds. It is also noteworthy that the data points for the compounds substituted in the para or ortho position by an electron-withdrawing group, **1‴**, **3**, **4**, and **5**, fall below this line with the two compounds bearing an ester group as para substituent being located on another 0.5 slope straight line situated 0.08 eV below the main line. The compound with a para cyano substituent is located 0.16 eV below the line and its ortho isomer, 0.12 eV. The pyridine compound, **8**, is located further below (at a distance of 0.22 eV from the main line).

It has been shown previously that the presence of electron-withdrawing groups in the para or ortho position of benzyl bromide and chloride decreases the bond dissociation energy substantially (by 0.25−0.30 eV) while electron-donating groups have little influence.[15] This effect has been interpreted as the result of a destabilization of the starting molecule (rather than of a stabilization of the benzyl radical) due to the opposing polarizations introduced by the electron-withdrawing substituent and the CH_2X group when they are located in resonance interacting positions.

We may therefore assign the downward location of **1‴**, **3**, **4**, and **5** in Figure 10a to the same destabilizing effect. The ortho cyano derivative **3** is located slightly above the para derivative **1‴** because of through-space effects in the former case. **4** and **5** are located above **1‴** because the electron-withdrawing power of ester substituent is less than with a cyano group. The strong electron-withdrawing power of the pyridine ring, explaining why **8** is located below all other compounds, matches the greater reducibility of the pyridine ring as compared to the benzene ring. Application of the linearized version of eqs [3] and [4] leads to estimating the decrease of the BDE of these compounds compared to that of the unsubstituted compound **7**, as 4/3 of the vertical distance between the two straight lines, i.e., 0.20, 0.16, and 0.10 eV, respectively. The same explanation holds for **8** with a larger distance, 0.22 eV, between the data point and the main line leading to a decrease of the BDE of 0.30 eV.

In this framework, the alignment of **2** and **9** with the unsubstituted compound **7** derives from the lack of resonance interaction between the electron withdrawing group (CN and pyridine) and the CF_3 group. In the case of **6**, the para effect observed with **1‴**, **3**, **4**, and **5** is counteracted by the negative charge borne by the carboxylate group.

The quantitative application of the intramolecular dissociative electron transfer model requires the estimation of the standard free energy of the cleavage reaction. This can be done, using eq 4, for the unsubstituted compound, **7**. The first term can be obtained as follows. We first estimated the bond dissociation energy of $PhCH_2-F$ from

$$D_{PhCH_2-F} = \Delta_f H_{PhCH_2\cdot} + \Delta_f H_{F\cdot} - \Delta_f H_{PhCH_2F} = 4.06 \text{ eV}$$

(the $\Delta_f H$'s are the enthalpies of formation of the subscript species) using literature data.[16]

We then assume that the increase of the BDE when going to the CHF_2 and CF_3 derivatives is the same as in *gem*-fluoralkanes.[14] Thus, $D_{PhCHF-F} = 4.18$ eV and $D_{PhCF_2-F} = 4.34$ eV. The last term in eq 4 represents the entropy increase corresponding to the formation of two particles out of one. Thus, ΔS is approximately 0.6 meV K^{-1} [10d] and the entropic term is 0.14 eV. The second term in eq 4 was determined experimentally. The last factor to be estimated is the standard potential for the oxidation of F^- in liquid NH_3 at 235 K. The standard potential at 298 K was derived according to the same procedure

(15) (a) Clark, K. B.; Wayner, D. D. M. *J. Am. Chem. Soc.* **1991**, *113*, 9363. (b) Andrieux, C. P.; Le Gorande, A.; Savéant, J. M. *J. Am. Chem. Soc.* **1992**, *114*, 6892.

(16) (a) Benson, S. N. *Thermochemical kinetics*; Wiley: New York, 1976. (b) *Handbook of Chemistry and Physics*, 72nd ed.; CRC: Cleveland, OH, 1991−1992.

Table 3. Standard Free Energies and Intrinsic Barrier Free Energies for the Cleavage of the Anion Radicals of 4-Cyanofluorotoluenes

medium		DMF at 20 °C		liquid NH_3 at −38 °C	
compd	BDE[a]	ΔG^{0} [a]	$\Delta G_0^{\ddagger}$ [a]	ΔG^{0} [a]	$\Delta G_0^{\ddagger}$ [a]
1′	3.86	−0.93	0.85	−1.35	0.91
1″	3.98	−0.68	0.75	−1.14	0.88
1‴	4.14	−0.41	0.805	−0.88	0.92
			0.805		0.90
			±0.05		±0.02

[a] In eV.

as already used for other anions.[17a] It was thus found that $E^{0,298\ K}_{F^{\bullet}/F^-,NH_3} = 3.33$ V vs 0.01 M Ag^+/Ag. The value at 235 K was then found to be $E^{0,235\ K}_{F^{\bullet}/F^-,NH_3} = 3.53$ V vs 0.01 M Ag^+/Ag.[17b]

Thus, $E^{0,235\ K}_{PhCF_3,NH_3} = -1.51$ eV. We may therefore recast the activation free energies of **2**, **6**, **7**, and **9** in a diagram having the reaction standard free energy as horizontal coordinate as shown in Figure 10b. Extrapolation of the 0.5 slope straight line to zero driving force thus provides the common value of the intrinsic barrier free energy, for these four compounds, $\Delta G_0^{\ddagger} = 0.96$ eV.

The data point for **1‴** is located 0.16 eV below the main correlation line in Figure 10a. As discussed earlier, this means that the bond dissociation energy of **1‴** is 0.20 eV smaller than that of the unsubstituted compound, **7**, i.e., $D_{\mathbf{1}'''} = 4.14$ eV. Thus from the application of eq [4], $\Delta G^0_{\mathbf{1}'''} = -0.88$ eV and, from the linearized version of eq [3], $\Delta G_0^{\ddagger} = 0.91$ eV. The contribution of the intramolecular dissociative electron transfer to the intrinsic barrier free energy may be estimated from eq [5] in the following manner. The anion of **1″**, produced in situ by deprotonation by *t*-BuO^-, gives rise, at a concentration of 3 mM and a scan rate of 0.2 V/s, to an irreversible cyclic voltammetric peak at 0.43 V vs 0.01 M Ag^+/Ag. In view of the values found for the heterogeneous rate constants found for the reduction of **1′**, **1″**, and **1‴**, and of the fact that the charge is more concentrated in the anion of **1″** than in the anion radicals of the preceding compounds, 0.1 cm s^{-1} is a reasonable estimate of the heterogeneous rate constant for the oxidation of the anion of **1″**. Assuming that the radical thus produced undergoes a rapid dimerization, the standard potential for this oxidation is very close to the peak potential (0.47 instead of 0.43 V vs 0.01 M Ag^+/Ag.).[11b]

It follows that $\Delta G^{\ddagger}_{0,intra}$ and therefore that $\Delta G^{\ddagger}_{0,solv}$. The possibility of an important contribution of solvent reorganization[18a] to the dynamics of intramolecular dissociative electron transfer has recently been demonstrated in the cleavage of anion radicals of α-substituted acetophenones.[10c,d]

Turning back to the di- and monofluoro compounds in the same series (Figure 9), we may estimate the reaction standard free energy in liquid NH_3 from the bond dissociation energies (Table 3) and the standard potentials (listed in Table 1). The intrinsic barrier free energy may then be derived from the application of the linearized version of eq 3 (Table 3). It is practically constant over the three compounds, **1′**, **1″**, and **1‴**. The constancy of this parameter points to the conclusion that the solvent reorganization energy is about constant and that the variations of the standard potentials for the oxidation of the carbanion (which both shift in the positive direction from **1′** to **1″** and **1‴**) compensate each other.

A similar analysis can be carried out for the results obtained in DMF with the same compounds. The standard potential for the oxidation of F^-, $E^{0,298\ K}_{F^{\bullet}/F^-,DMF} = 2.59$ V vs SCE, was obtained from the available free energy of transfer from water to DMF.[17c,d] The values of the reaction standard free energies and intrinsic barrier free energies ensue (Table 3). The intrinsic barrier free energy is again *ca.* constant over the series pointing to the same conclusions as in liquid NH_3.

We also note that the intrinsic barrier free energies are not very different when going from liquid NH_3 at −38 °C to DMF at room temperature. It follows that the increased cleavage reactivity observed in the former case as compared to the latter is essentially caused by an increase of the driving force. This is itself mainly due to a better solvation of the leaving fluoride ion by the protic solvent NH_3 as compared to the aprotic solvent DMF. For the following reasons, the intrinsic barrier is however not strongly affected by this variation of the anion solvating properties. Both $E^0_{RX/RX^{\bullet}}$ and $E^0_{R^{\bullet}/R^-}$ in eq 5 are expected to shift in the negative direction when passing from liquid NH_3 to DMF, the latter factor more than the former (because the negative charge is more concentrated in R^- than in $RX^{\bullet -}$). The ensuing increase of the intrinsic barrier is however compensated by a decreased solvent reorganization energy.[18]

Conclusions

1. The reductive cleavage of the trifluoromethylarenes leads to completely defluorinated products. It goes through the intermediate formation of the difluoro and monofluoromethyl derivatives. The monofluoromethyl derivative is likewise an intermediate in the reduction of aryldifluoromethyl compounds. Unlike *gem*-dichloro, dibromo, or chloro−bromo compounds, carbenes are not formed along the reaction pathway. The reaction involves fluoride expulsion from the primary anion radical, followed by reduction of the neutral radical thus formed. The resulting carbanion rapidly protonates, thus producing the hydrogenolysis product, rather than cleaving off a fluoride ion to form a carbene. The difference with the chloro and bromo analogues is presumably caused by the fact that carbon−fluorine bonds are much stronger than with the other halogens

2. The standard potential for the formation of the anion radical increases from the mono to the di- and the trifluoro derivatives. The three standard potentials are however closely spaced, thus opening the possibility of an internal redox catalysis leading to an apparent direct six-electron reduction of the three C−F bonds. The occurrence of such a mechanism depends upon the stability of the primary anion radical toward cleavage. It is followed, as demonstrated on quantitative grounds, when cleavage of the primary anion radical is slow enough for the resulting radical to be formed far from the electrode surface. Then, the product in which one fluorine has been replaced by one hydrogen is itself formed far from the electrode surface and undergoes homogeneous electron transfer from the primary

(17) (a) See Table 2 in ref 9a and the references quoted therein. (b) $E^{0,235\ K}_{F^{\bullet}/F^-,NH3} - E^{0,298\ K}_{F^{\bullet}/F^-,NH3} = (298 - 235)(S^0_{F^{\bullet}} - S^0_{F^-,NH3} - S^0_{Ag^+,NH_3} + S^0_{Ag})$ (the S^0's being the entropies of formation). $S^0_{F^{\bullet}} = 1.65$, $S^0_{Ag} = 0.44$ meV K^{-1}.[16b] The entropies of formation of F^- and Ag^+ in liquid NH_3 were derived from their values in water (−0.14 and 0.76 meV K^{-1} respectively[16b]) by means of: $S^0_{F^-\ or\ Ag^+,NH_3} = S^0_{F^-\ or\ Ag^+,H_2O} + \Delta_{tr}S_{F^-\ or\ Ag^+,H_2O\rightarrow NH_3}$ (the $\Delta_{tr}S$ are the entropies of transfer). $\Delta_{tr}S_{Ag^+,H_2O\rightarrow NH_3} = -0.26$ meV K^{-1}.[17c] For F^-, we used the following procedure in the absence of directly available data. There is a good linear correlation between the entropies of transfer of Cl^-, Br^-, and I^- from H_2O to NH_3 and from H_2O to $HCONH_2$: $\Delta_{tr}S_{X^-,H_2O\rightarrow NH_3} = 1.52\Delta_{tr}S_{X^-,H_2O\rightarrow HCONH_2} - 1.18$ meV K^{-1}.[17d] Extrapolating for F^- we obtained, using $\Delta_{tr}S_{F^-,H_2O\rightarrow HCONH_2} = -0.12$ meV K^{-1},[17d] $\Delta_{tr}S_{F^-,H_2O\rightarrow NH_3} = -1.36$ meV K^{-1}. Since $S^0_{F^-,H2O} = -0.14$ meV K^{-1},[17d] $S^0_{F^-,NH3} = -1.50$ meV. (c) Marcus, Y. *Pure Appl. Chem.* **1985**, *51*, 1103. (d) Marcus, Y.; Kamlet, M. J.; Taft, R. W. *J. Phys. Chem.* **1988**, *92*, 3613.

(18) Eq 6, being based on a Born model of solvation, is likely to be a rather poor representation of the differences between a H-bonding solvent and an aprotic solvent although the predictions deriving from the size of the charge location volume and to the center-to center distant are most likely correct.

anion radical before having time to diffusing back and being reduced at the electrode surface. For these reasons, this "disproportionation" or internal redox catalysis mechanism occurs with trifluoro derivatives bearing electron-withdrawing groups on the aromatic moiety. Conversely, an "ECE" mechanism, where the defluorinated intermediate being formed close to the electrode surface undergoes an electrode electron transfer, occurs with trifluoro derivatives bearing an electron-donating substituent or no substituent at all as well as with the difluoro derivatives.

3. The variations of the cleavage reactivity with the number of fluorines on the functional carbon and with the structure of the aromatic moiety were derived from cyclic voltammetric and/or redox catalysis experiments. They could be successfully rationalized by the intramolecular dissociative electron transfer model. Application of the model involves relating both the driving force (the opposite of the standard free energy of the reaction) and its intrinsic barrier to structural and medium factors in the reactants and products.

4. The rate of anion radical cleavage increases rapidly from the trifluoro to the difluoro and to the monofluoro derivative. In terms of driving force, an important factor is the standard potential for the generation of the anion radical (E^0) which measures the LUMO energy. The higher the later factor, the larger the driving force, and thus, the faster the reaction. The acceleration of the reaction indeed parallels a shift of the standard potential in the negative direction. This is however insufficient to account quantitatively for the magnitude of the acceleration. One should take into account the variation of another factor, namely the homolytic bond dissociation energy of the starting molecule (D) which decreases as the number of fluorines diminishes. This is a second reason why the driving force increases from 3 to 2 and to 1 fluorines. This factor also influences the intrinsic barrier, which decreases as the number of fluorines diminishes. On total, the activation free energy correlates, as predicted by the intramolecular dissociative electron transfer model, with $E^0/2 + 3D/4$. This correlation implies that the sum of the other ingredients of the intrinsic barrier remains constant in the series. This constancy derives from the approximate constancy of the solvent reorganization energy and from the fact that the variations of the standard potentials for the formation of the anion radical and for the oxidation of the defluorinated carbanion compensate each other while shifting in the negative direction upon passing from 3 to 2 and to 1 fluorines.

5. The standard potential for the formation of the anion radical of the trifluoro derivatives varies substantially upon changing the aryl moiety. This is the main factor which makes the cleavage rate constant vary in the series through the ensuing variation of the driving force. The bond dissociation energy of the starting molecule also interferes both in the driving force and in the intrinsic barrier. This is the reason that the presence of an electron-withdrawing substituent, when located in a resonant interacting position with the CF_3 group, accelerates the cleavage reaction by means of the attending weakening of the C−F bond.

6. The activation free energy of cleavage is smaller in liquid NH_3 at −38 °C than in DMF at room temperature. This difference in reactivity is essentially of thermodynamic origin. It derives from a better solvation by NH_3 (H-bonding solvent) than by DMF (non H-bonding solvent). In both solvent the major contribution to the intrinsic barrier comes from the nuclear reorganization attending the intramolecular dissociative electron transfer. However solvent reorganization is far from negligible. Its contribution to the intrinsic barrier is *ca.* one-third of the total. The fact that the intrinsic barrier free energy is approximately the same in both solvents results from the compensation of two effects. Passing from DMF to liquid NH_3 shifts the standard potentials for the formation of the anion radical and for the oxidation of the defluorinated carbanion both in the positive direction; the later more than the former because the negative charge it bears is concentrated over a smaller volume. The resulting decrease of the intrinsic barrier is however compensated by an increase of the contribution of solvent reorganization.

Experimental Section

Cyclic Voltammetry. In liquid NH_3, the working electrode was a 0.5 mm-diameter gold disk, frequently polished with alumina. A platinum wire was used as counter electrode, and the reference electrode was a 0.01 M Ag^+/Ag electrode.[19a] The potentiostat, equipped with a positive feedback compensation and current measurer,[19b] was used together with a function generator (Tacussel TPPRT), a storage oscilloscope (Nicolet), and an X-Y recorder (Sefram TGM164). The cyclic voltammetry experiments were run in an electrochemical cell[19c] filled with 80 mL of liquid ammonia, and potassium bromide was used as supporting electrolyte. The temperature was maintained at −38 °C with a cryostat (Bioblock Scientific).

In DMF, the working electrodes were 1 or 3 mm diameter carbon disks. They were carefully polished and ultrasonically rinsed with ethanol before each voltammogram. The counter electrode was a platinum wire and the reference electrode an aqueous SCE electrode. The potentiostat, function generator, and recorders were the same as above. The experiments were carried out at 20 °C in an electrochemical cell equipped with a double-wall jacket allowing circulation of water filled with 5 mL of DMF and *n*-Bu_4NBF_4 as supporting electrolyte.

Chemicals. *N*,*N*′-Dimethylformamide (Fluka puriss absolute) and the supporting electrolyte *n*-Bu_4NBF_4 (Fluka puriss) were used as received.

All trifluoro compounds, with the exception of **5** and **6**, were purchased from Aldrich or Maybridge.

5 was prepared according to literature[20a] from the corresponding benzoic acid chloride and *t*-BuOH. A white solid is obtained after separation of the reacting mixture is separated on a silica column. with a 70−30 cyclohexane−dichloro methane mixture as eluant. Yield: 56%; ^{1}H NMR ($CDCl_3$) δ 1.62 (s, 9 H), 7.71−8.14 (AA′BB′, J_{AB} = 9Hz, 4H); ^{13}C NMR ($CDCl_3$) δ 28.1 (CH3), 80.8 (C), 123.5 (CF3, q, J_{CF} = 272 Hz), 125.3 (CH, q, J_{CF} = 4 Hz), 129.8 (CH), 133.2 (C), 134.3 (C, q, J_{CF} = 32.5 Hz), 165.7 (C).

6 was prepared *in situ* by addition of a stoichiometric quantity of *t*-BuOK to the acid.

To obtain **1″**,[20b] a mixture of 4-cyanobenzaldehyde (5 mmol) and diethylaminosulfur trifluoride (5.2 mmol) was heated carefully till the start of the exothermic reaction. It was then maintained at 60 °C for 30 min. The resultant mixture was dissolved in dichloromethane (15 mL), and the solution was poured into ice (20 mL) to remove the diethylamino-*N*-sulfinyl fluoride formed in the reaction. The organic layer is dried with magnesium sulfate. The products are eluted with dichloromethane on a silica column. A pale yellow liquid is obtained after evaporation of the eluant. Yield: 79%; ^{1}H NMR (CD_3COCD_3) δ 6.70 (t, J_{HF} = 56 Hz, 1 H), 7.65−7.78 (AA′BB′, J_{AB} = 8.3 Hz, 4 H); MS: *m*/*z* 153 (M), 152 (M − 1), 134, 103.

To prepare **1′**,[20c] 5.5 mmol of 4-bromomethylbenzonitrile were added to 10 mL of a THF solution of NBu_4F (1 M). The mixture was stirred under an inert atmosphere at ambient temperature during 20 h. The resultant mixture was poured in pentane (15 mL) and washed 3 times with water (10 mL). The organic layer was dried with magnesium sulfate, and the products separated on a silica column with CH_2Cl_2 as eluant). A pale yellow liquid was finally obtained (mp ≈ 25 °C).

(19) (a) Herlem, M. *Bull. Soc. Chim. Fr.* **1967**, 1687. (b) Garreau, D.; Savéant, J.-M. *J. Electroanal. Chem.* **1972**, *35*, 309. (c) Combellas, C.; Lu, Y.; Thiébault, A. *J. Appl. Electrochem.* **1993**, *23*, 841.

(20) (a) Furniss, B. S.; Hannaford, A. J.; Smith, P. W. G.; Tatchell, A. R. *Vogel's Textbook of Practical Organic Chemistry*, 5th ed.; Longman, Ed.; Essex UK, 1989; pp 1073−1081. (b) Markovskij, L. N.; Pashinnik, V., E.; Kirsanov A. V. *Synthesis* **1973**, 787. (c) Cox, D. P.; Terpinski, J.; Lawrynowicz, W. *J. Org. Chem.* **1984**, *49*, 3216.

Yield: 85%; ^{1}H NMR (CD_3COCD_3) δ 5.63 (d, J_{HF} = 45 Hz, 2H), 7.63−7.84 (AA′BB′, J_{AB} = 9 Hz, 4H); MS: *m*/*z* 135 (M), 134 (M − 1), 110, 108, 107.

Attempted Trapping of Carbene Intermediates. Experiment 1. Compound **1‴** (3 mmol) and 2,3-dimethyl-2-butene (20 mmol) were introduced into an electrochemical cell containing 20 mL of acetonitrile and NBu_4BF_4 (0.1 M) as supporting electrolyte. The cathode (a 4 cm^2 stainless steel foil) and the anode (1 cm diameter magnesium rod) were then introduced in the reactor, and the electrolysis was performed under controlled current density (0.7A dm^{-2}). It was stopped after the consumption of 3 Faradays per mol of substrate. The products were extracted with dichloromethane, thoroughly washed with water, and then analyzed by GC/MS. Analysis of products gave 39% 4-toluonitrile and 61% unreacted **1‴**.

Experiment 2.[13a] **1″** (0.7 mmol) and *t*-BuOK (0.9 mmol) were added, under controlled atmosphere, to 2,3-dimethyl-2-butene (8.5 mmol). The mixture rapidly turned brown, and it was stirred for 24 h. The mixture was then dissolved in dichloromethane and poured into water. The organic layer was dried over magnesium sulfate and then analyzed by GC/MS. Starting products were recovered without formation of cyclopropanic product.

Supporting Information Available: Figures S1−S4 summarize the i_p/i_p^0 data and the procedure for extracting the rate constants from them (2 pages). See any current masthead page for ordering and Internet access instructions.

JA971094O